2007 IEEE International Conference on
Robotics and Automation
Roma, Italy, 10-14 April 2007

Granular Space Structure on a Micrometric Scale for Industrial Robots

Jean-François Brethé and Dimitri Lefebvre

Abstract– **We study the statistical relationship between angular position and target for industrial robots on a micrometric scale and this leads us to understand the angular position stochastic structure. The concept of granular angular space is introduced and transposed in the Cartesian space. Modeling is based on experimental work performed for a Kuka and a Samsung robot. The influence of workspace location, posture and angular granularity ratio on the Cartesian granular space are then analysed.**

I. INTRODUCTION

In the field of industrial robots, repeatability and precision are two different concepts. Repeatability measures the dispersion between final points when the target is the same and the move is repeated several times. Precision is the distance between the mean of points and the target as explained in ISO9283 [8]. Modellings of repeatability phenomena for industrial robots exist [7], [10] and influence of workspace location, load and speed on repeatability were studied [11], [9]. We proposed a new modelling based on stochastic ellipsoids which takes into account workspace location and load [1]. This theory is briefly explained in section II and was validated on a Kuka robot [5]. The aim of the paper is to explore the consequence of this modelling for the stochastic structures of both angular and Cartesian spaces. In section III, the structure of angular space is detailed and the concept of granularity ratio introduced. In section IV, the resulting stochastic structure in the Cartesian space is described. In section V, the influence of granularity ratio is analysed and in section VI, we study how redundancy affects the stochastic structure.

II. STOCHASTIC ELLIPSOID THEORY

We now outline the stochastic ellipsoid theory detailed in a previous paper [2].

In the formula $X = f(\Theta)$, the forward kinematics function of a robot transforms joint coordinates $\Theta = (\theta_1, ..., \theta_6)$ into workspace coordinates $X = (x, y, z)$. The Jacobian function maps the joint velocity vector to the Cartesian velocity vector in the linear transformation $dX = J(\Theta)d\Theta$. This relationship can also be understood as the link between small angular and Cartesian variations.

The angular variation $d\Theta$ can be modelled with a Gaussian distribution [4]. As the 6 axes have independent control, the angular position random variables are independent. So $d\Theta$ is a Gaussian vector whose covariance matrix D can be determined using our experimental procedure.

J.-F. Brethé and D. Lefebvre work in GREAH, Le Havre University, France. Email to jean-francois.brethe@univ-lehavre.fr

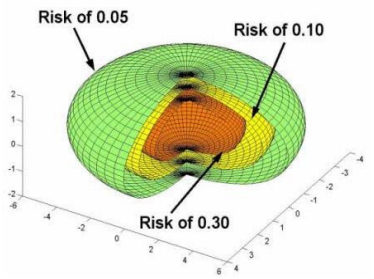

Fig. 1. Representation of stochastic ellipsoids associated with different risks

The theory of Gaussian vectors then indicates that dX is also a Gaussian vector whose covariance matrix is $C = J \times D \times J^T$ [12]. The density g of the position vector is the following : $g(dX) = k \exp\left[-\frac{1}{2} dX^T C^{-1} dX\right]$ where the constant k is computed by normalizing the density function $\iiint_{\Re^3} k \exp\left[-\frac{1}{2} U^T C^{-1} U\right] dU = 1$.

The isodensity surfaces are ellipsoids generated by the equation $dX^T C^{-1} dX = Cst$, named "stochastic ellipsoids". The reference stochastic ellipsoid is determined from the equation $dX^T C^{-1} dX = 1$.

Each ellipsoid is associated with a level of risk; the risk is the probability that the point will fall outside the ellipsoid. Fig. 1 displays three ellipsoids associated with different levels of risk.

It is possible to draw reference stochastic ellipsoids in different locations in the workspace. Then, using a central homothety we can build stochastic ellipsoids with different levels of risk.

The main axes of the reference stochastic ellipsoid are the eigenvectors of the covariance matrix C and the lengths of the semi-axes are the square root of the eigenvalues of the covariance matrix C.

To sum up, the cloud of points associated to every target in the workspace is enclosed in a stochastic ellipsoid. Of course, the size, orientation and eccentricity of the stochastic ellipsoid is different depending on workspace location.

III. ANGULAR RESOLUTION AND $\sigma-$INTERVALS

In this section the relation between the encoder resolution, the control and the angular position covariance matrix are discussed. The theoretical modelling is then illustrated for two different robots.

A. Control, encoder resolution and covariance matrix

In the control process of a robot actuator, the difference between the target which is a number, and the real final position should be nil. Several parameters intervene in the global control accuracy : for instance, target resolution, which is the smallest difference taken into account by the controller, encoder resolution, internal control process accuracy... As the final position depends on all these factors, we chose in a pragmatic way, to study the link between the target and the measured angular positions. Axis standard deviation lies in the angular covariance matrix previously introduced. The purpose is now to study the stochastic structure of angular space, particularly the distance between the two closest angular position distributions.

B. Target, $\sigma-$Intervals and granularity ratio

Let us study the relation between the values of the target T_n, T_{n+1},... and the measured angular positions of the actuator X_n, X_{n+1},.... Let Δ be the target resolution i.e. the difference between two nearest targets T_n and T_{n+1} which can be entered in the controller. The positions of the random variables X_n and X_{n+1} associated with the targets T_n and T_{n+1} are measured and a statistical analysis is performed to estimate the position distributions, in particular the means $\overline{X_n}$ and $\overline{X_{n+1}}$. The standard deviation σ of the two random variables X_n and X_{n+1} is the same.

The angular distribution is modelled with a normal density[3]. An important consequence is that the two distributions X_n and X_{n+1} have a non-empty intersection. This means that some areas can be attained from two different targets even if the robot is non-redundant. This could be a problem, but in practice, the probability of this event is very low !

It is interesting to draw a typology of angular space stochastic structure. The confidence interval I_n can be used for this purpose. The length of the intervals depends then on the standard deviation σ so let us call them $\sigma-$intervals. For instance, the 99.7% confidence interval is a $6\sigma-$interval .

The stochastic structure of the angular space depends then on the relative positions of I_n and I_{n+1}. Three different cases may occur as illustrated in fig. 2 :

1. There is a gap G_n between I_n and I_{n+1} : this means that it is impossible to attain some sets of angular positions. There are some holes in the stochastic structure of the angular space.

2. The intervals I_n and I_{n+1} have a non-empty intersection K_n. This definitely means that there are at least two different targets that could put X in K_n. This is a crucial problem because it could lead to major micrometric non-linearities.

3. The intervals I_n and I_{n+1} are contiguous. The space is paved with $(I_n)_{n\epsilon\mathbb{N}}$ The result is much better because every interval is associated with only one target. Non-linearities have not disappeared but are reduced to their smallest possible size. They subsist within the interval I_n itself.

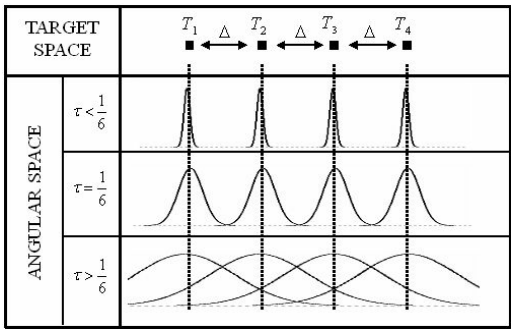

Fig. 2. Typology of angular stochastic structure depending on the granularity ratio τ

The different cases of this typology can be classified using the ratio $\tau = \frac{\sigma}{|\overline{X_n}-\overline{X_{n+1}}|}$ for a given risk α. For instance, in this paper let $\alpha = 0,003$; if $\tau = \frac{1}{6}$ then the intervals are contiguous ; if $\tau < \frac{1}{6}$ then some holes appear and if τ is very small, it is as if there were some aggregates in angular space ; if $\tau > \frac{1}{6}$ then the intervals are intersecting. For these reasons, we propose to define τ as the granularity ratio.

C. Granularity ratio determination

The following experimental procedure is used to obtain the σ interval for an industrial robot and is applied to one axis at a time. For the i-th axis, the target cycle is the following $T_0 \rightarrow T_1 \rightarrow T_0$ then $T_0 \rightarrow T_1 + \Delta \rightarrow T_0$ then $T_0 \rightarrow T_1 + 2\Delta \rightarrow T_0$ etc. This cycle is repeated at least 25 times. This solution has been preferred to the one which consisted of achieving first 25 times the cycle $T_0 \rightarrow T_1 \rightarrow T_0$ then 25 times the cycle $T_0 \rightarrow T_1 + \Delta \rightarrow T_0$ etc. Indeed, we observed experimentally there was a drift which biased significantly the results of the second procedure. Conversely, in the first procedure, the drift influence is equally divided between every target so the determination of the difference between the means is not affected.

The positions $X_1(n), X_2(n), X_3(n), X_4(n)$ corresponding with the targets $T_1, T_1+\Delta, T_1+2\Delta, T_1+3\Delta$ are measured using Mitutoyo micrometers. Their precision is higher than 3 μm. The micrometer is set on a system of Microcontrol beams assuring stability. The difficulty is to move one actuator at a time which implies low speed to avoid dynamic efforts.

In this methodology, the internal process of the robot actuator controller is not taken into account. The real and effective changes in positions are observed and measured. As this distribution is normal, it will be characterized by the mean and variance.

The procedure is carried out on a Kuka robot (fig. 3) and a Samsung robot (fig. 4) leading to the following results.

1) The Kuka Robot: For the Kuka robot first axis, the trajectories are illustrated in fig.5. First, it is interesting to notice that the four trajectories do not intersect, except at one point. There is still a gap between the different measured

Fig. 3. "IR364" Kuka Robot Structure

Fig. 4. "Faraman" Samsung Robot Structure

positions associated to different targets. The mean of two consecutive trajectories $X_k(n)$ and $X_{k+1}(n)$ is estimated and the results are very close whatever the value of k is as detailed in table I : $\delta = 0.018$ mm. The standard deviation is estimated via the jump process $J_k(n+1) = X_k(n+1) - X_k(n)$ to eliminate the drift influence [5]. The standard deviation of X_k is equal to the standard deviation of J_k divided by $\sqrt{2}$ which gives $\sigma = 0.0076$ mm. The granularity ratio is then $\tau = 0.41$.

The stochastic structure is similar for the second and third axis : the distance between the mean positions $\overline{X_n}$ and $\overline{X_{n+1}}$ is almost the same. The granularity ratio increases slowly to 0.52.

From the fourth axis to the sixth axis, the stochastic structure is more complex. The length between $X_{k+1}(n)$ and $X_k(n)$ depends on k. This is illustrated by fig. 6 and table I.

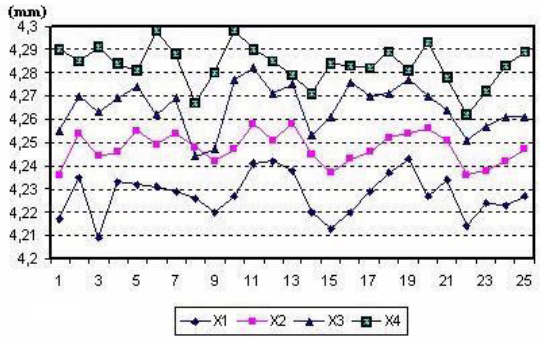

Fig. 5. Kuka robot first axis trajectories

TABLE I

DISTANCE BETWEEN MEANS FOR THE KUKA ROBOT

Location	$X_1 \rightarrow X_2$	$X_2 \rightarrow X_3$	$X_3 \rightarrow X_4$
distance 1st axis (mm)	0.0199	0.0176	0.0181
distance 4th axis (mm)	0.0056	0.0038	0.0084

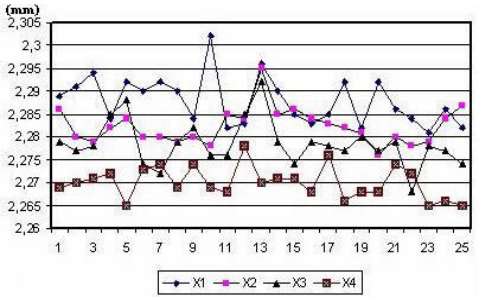

Fig. 6. Trajectories for Kuka Robot Fourth axis

In more than 15 cases, the trajectories often overlap. If the target was increased in one direction, the measured position difference was in the other direction which is an obvious non-linearity.

For the last three axes corresponding to the wrist, the granularity ratio increases consequently as detailed in table II. So it is more and more difficult to decipher the trajectories and control the robot in the micrometric local space to avoid non-linearities.

2) The Samsung Robot: The behavior of the Samsung robot Faraman is quite different from the Kuka robot. First, the target resolution is 0.01 for the Samsung and 0.001 for the Kuka. Repeating the same protocol as for the Kuka, we noticed that for the Samsung robot, the gap between two trajectories is very wide as illustrated in fig. 7 which displays the phenomenon for the first axis. The same phenomenon is observed for the six axes of the robot.

The granularity ratio is very low in the range from 1.5% to 7.9% as detailed in table II. This means that the control of the robot is not optimized. The controller resolution seems to be

TABLE II

GRANULARITY RATIOS FOR KUKA AND SAMSUNG ROBOT

Axis	1st	2nd	3rd	4th	5th	6th
Kuka ratios	0.41	0.48	0.52	0.73	0.74	1.10
Samsung ratios	0.01	0.02	0.02	0.04	0.05	0.07

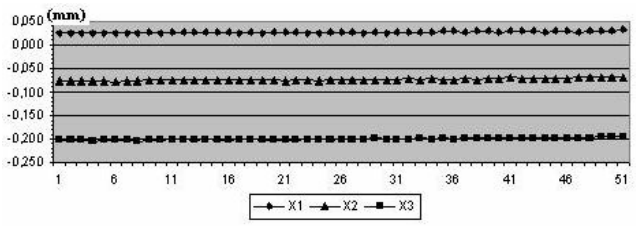

Fig. 7. Samsung robot first axis trajectories

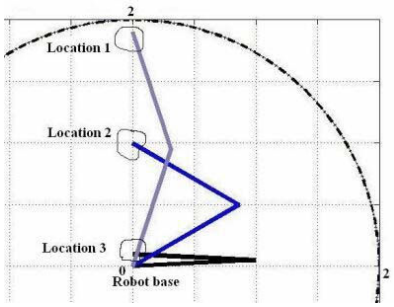

Fig. 8. SCARA2 and some specific locations

much better than the target resolution and as the repeatability is very good, there are large areas that are unattainable in the angular space. If the target resolution was 0.001 for instance, the gap between two nearest angular position would be narrower and the resolution would be better in the angular space.

As a conclusion, the two robots Kuka and Samsung have a completely different angular stochastic structure in the typology we defined. For the Samsung it is like the structure $\tau < \frac{1}{6}$ of fig. 2 whereas for the Kuka it corresponds to the case $\tau > \frac{1}{6}$.

IV. Analysis of Granular Space Structure of SCARA2

In this section, we suppose $\tau = \frac{1}{6}$ so that the angular stochastic structure is contiguous. We investigate the resulting stochastic structure in Cartesian space, by considering, for simplicity, a SCARA2 robot with two axes controlled by the angles (θ_1, θ_2). The lengths of the two arms are the same. Three workspace locations are chosen to analysis the evolution of the Cartesian space stochastic structure (fig. 8). They are typical of the different structures that can be observed.

For the SCARA2, the target is a pair of angles (θ_1, θ_2). Let (Δ_1, Δ_2) be the target resolution on the first and second axis. A stochastic ellipse is associated to every target. Let the center position of one ellipse be known and let us draw the other ellipses closest to the first one. The centers of the surrounding ellipses are at a distance :

$$J(\theta_1, \theta_2) \times (k\Delta_1, p\Delta_2)^t$$

where $(k, p) \in \mathbb{Z}^2$, $J(\theta_1, \theta_2)$ is the Jacobian matrix. Let us draw different ellipses when $\Delta_1 = \Delta_2 = 0.06\ rad$. The resulting structure is illustrated in fig. 9.

At first glance, as the scale of local space is the same for the three locations, we notice that the disposition, size and eccentricity of the ellipses are completely different. The surface of the stochastic ellipses are considerably smaller in the first location compared to the others. Let us analyse more precisely the differences and the consequences for micrometric repositioning behavior.

In the first location, ellipses have a high eccentricity of nearly 10 and are positioned on a regular rectangular mesh.

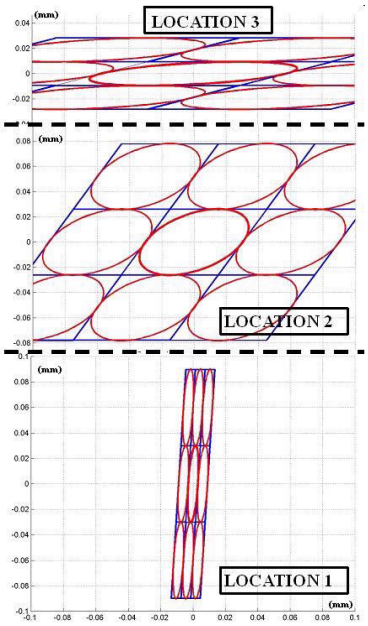

Fig. 9. Stochastic structure of Cartesian space for the SCARA2 at specific locations

Using a different target, it is possible to correct the position with a higher precision in the x-direction than in the y-direction. The spatial resolution is better in the x-direction. Adding $(\Delta_1, 0)$ to the target produces an average move of 0.006 mm in the x-axis ; but adding $(0, \Delta_2)$ to the target gives an average displacement of 0.06 mm in the y-axis. So it is easier to control the position in the x-axis direction. Of course it is not a direct displacement which would be impossible because of friction, but it implies returning to the initial posture and coming back with a slightly different target.

Another important conclusion is that it is nearly impossible to reach the holes between ellipses ; the probability is very low. Conversely, the chances of reaching a small area are higher as this area is situated near the centre of an ellipse. It means that the Cartesian space has a "granular stochastic structure" : there are some areas you have no chance of going to and some areas where the robot is attracted which are called aggregates. That is a very important result for the micrometric behavior of the robot and it explains most of the observed non-linearities.

For the second location, the eccentricity is around two, i.e. the major axis length is twice the minor axis length. The mesh is not rectangular any more but is based on parallelograms. Here again the granular stochastic structure is present with holes and granularities, corresponding to low and high probability density values. Modifying the target, it is possible to change average position by 0.06 mm in the x-direction and by 0.06 mm in the y-direction but the corrections are not always independent. A correction of 0.06 mm in the x-direction is possible keeping the same y-value. But a correction of 0.06 mm in the y-direction will produce an average displacement of 0.03 mm in the x-direction.

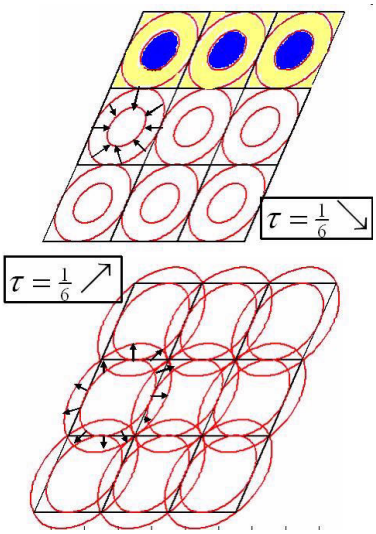

Fig. 10. Evolution of workspace granularity with the angular space granularity ratio

This is the case because there is a correlation in x- and y-displacements.

For the third location, eccentricity is high, nearly 6, and ellipses are meshed in a different way. Ellipses are intertwined so the x- and y- spatial resolutions are dependant. For instance, a new target can correct the x-position in two different ways: either the same y-position is to be kept, and the average displacement in x will be 0.12 mm ; or a small displacement in y of 0.02 mm is acceptable, and then the smallest displacement in x will be only 0.06 mm.

These different situations for a very simple assembly robot illustrate clearly the concept of "granular stochastic structure". The cartesian space has holes and aggregates, meaning areas with low or high positioning probabilities and this is essential to understand robot micrometric behavior and be able to control it better.

V. Influence of Granularity Ratio

In the preceding section, the granularity ratio was $\tau = \frac{1}{6}$ and the resulting stochastic structure for the two axes was displayed in fig. 9. Let us detail what happens if the granularity ratio of the angular actuator distribution is different. Ellipses are drawn for the SCARA2 robot in location 2. The resulting structures are detailed in fig. 10.

When the granularity ratio drops and this means $\tau \ll \frac{1}{6}$, stochastic ellipses contract. As a consequence, the volume of unattainable space increases and the final position is concentrated in small and easy to attain areas. This seems to be very interesting but there is a drawback : if the small area you want to go to is outside one aggregate position, you have no chance of going there.

On the other hand, when the granularity ratio increases and this means $\tau \gg \frac{1}{6}$, ellipses are larger and their edges are outside the mesh. As a consequence, in the stochastic space, the contrast between holes and aggregates lowers. This means that every point in the workspace is in theory accessible but the probability of reaching them decreases as the granularity ratio increases. So in practice several attempts are necessary to get there.

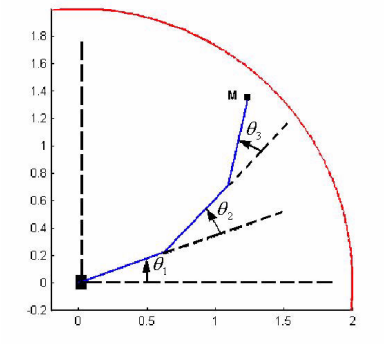

Fig. 11. Redundant SCARA3 robot

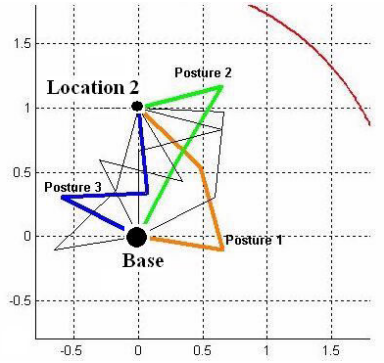

Fig. 12. Three different postures in location 2 for SCARA3

VI. Influence of Redundancy

In this section, the influence of redundancy on the stochastic structure of the Cartesian space is studied via a planar SCARA3 robot with three links of the same length and three actuators displayed in fig. 11.The granularity ratio is $\tau = \frac{1}{6}$ for the 3 axes and the target resolution is identical to the SCARA2.

The lengths of the three arms are chosen equal and the workspace surface is the same as the SCARA2. The stochastic structure is detailed in location 2 for three different postures described in fig. 12.

Fig.13 reveals the positions of some aggregates for the first, second and third posture. To keep the figures readable, only one ellipse is represented and the others are just positioned by their centers. But for a given posture, all ellipses are locally of the same size and orientation.

For a given location in the workspace, there is one mesh for the stochastic ellipse center positions for the SCARA2 which was described in fig. 9. But, for the SCARA3, the stochastic structure of Cartesian space depends on the posture of the robot. First, the main features of the stochastic ellipses are not the same : surface, orientation and eccentricity are slightly different. Then, the mesh of the stochastic ellipse center positions are not the same. Comparing SCARA2 and

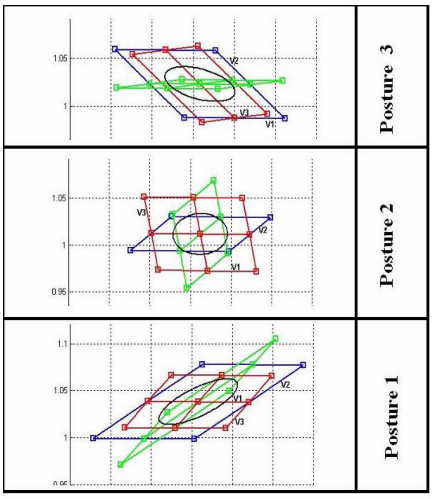

Fig. 13. Positions of aggregate centers in the Cartesian stochastic space for three different postures of SCARA3

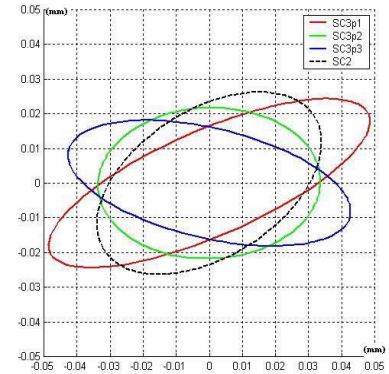

Fig. 14. Comparison of stochastic ellipses for SCARA2 and 3 postures of SCARA3

SCARA3 workspace stochastic structures, the conclusion is that they differ mainly from the local density of the ellipse center: a given surface in the local workspace encloses more SCARA3 ellipses than SCARA2 ellipses. As a consequence, the SCARA3 is easier to manoeuvre in the local micrometric space. Changing the target slightly will change the mean position slightly. On the contrary, if the SCARA2 target is slightly changed, the resulting displacement will be steeper.

Fig. 14 compares the surface and the orientation of the stochastic ellipses for these 3 postures of SCARA3 robot and for also SCARA2. It is obvious than the major differences in the stochastic structure do not lie in the surfaces or orientations of the stochastic ellipses because they are relatively the same. But the difference lies in the way the ellipse centers pave locally the Cartesian workspace. We have a paving of separated stochastic ellipses for the SCARA2 robot, and for the SCARA3, ellipses have a non-empty intersection

So the redundant SCARA3 robot has a better spatial resolution. It is better to use a redundant robot to manoeuvre in a micrometric local space but it implies of course a greater effort in the choice of the corrected target.

VII. Conclusions

In this paper, we first outlined stochastic ellipsoid modelling then introduced the concept of granular stochastic structure for angular distribution. The distance between the two closest targets in the controller is called the target resolution and the link between target resolution and angular granular stochastic structure is detailed. We defined a granularity ratio and drew up a typology of granular stochastic structures. The modeling was applied to two industrial robots, a Kuka and a Samsung.

Then, we tried to analyse the Cartesian stochastic structure resulting from the angular granular structure. First for a SCARA2 robot, we studied the influence of workspace location and granularity ratio. Finally, the case of a redundant SCARA3 robot is analysed, showing that it was better at manoeuvring in the local micrometric space.

As a conclusion, a detailed analysis of the stochastic structure of micrometric Cartesian space is carried out. It explains most of the non-linearities observed experimentally and this modeling will be used in our future work to develop a more precise local repositioning, trying to reach a high level of precision in the micrometric local space.

References

[1] Jean-François Brethé. "Contribution à la modélisation de la répétabilité des robots manipulateurs par les ellipsoïdes stochastiques". PhD thesis, Université du Havre (2004).

[2] Jean-François Brethé and Brayima Dakyo. A stochastic ellipsoid approach to repeatability modelisation of industrial robots. In "IROS02", pages 1608–1613. EPFL-Lausanne (2002).

[3] Jean-François Brethé, Eric Vasselin, Dimitri Lefebvre, and Brayima Dakyo. Validation expérimentale du modèle des ellipsoïdes stochastiques pour la répétabilité d'un robot kuka. In "JNRR03". LASMEA-Clermont-Ferrand (2003).

[4] Jean-François Brethé, Eric Vasselin, Dimitri Lefebvre, and Brayima Dakyo. Determination of the repeatability of a kuka robot using the stochastic ellipsoid approach. In "ICRA05", pages 4350–4355. CIMNE-Barcelone (2005).

[5] Jean-François Brethé, Eric Vasselin, Dimitri Lefebvre, and Brayima Dakyo. Modelling of repeatability phenomena using the stochastic ellipsoid approach. In "Robotica", volume 24, pages 477–490 (2006).

[6] Jean-François Brethé, Eric Vasselin, Dimitri Lefebvre, and Brayima Dakyo. Modélisation spatio-temporelle de la répétabilité des robots manipulateurs par les ellipsoïdes stochastiques. In "CIFA06". LAPS-Bordeaux (2006).

[7] Yael Edan, Lea Friedman, Avraham Mehrez, and Leonid Slutski. A three-dimensional statistical framework for performance measurement of robotic systems. In "Robotics and Computer-Integrated Manufacturing", volume 14, pages 307–315 (1998).

[8] ISO. "Manipulating Industrial Robots - Performance criteria and related test methods". ISO (1998).

[9] O. Felix Offodile and Kingsley Ugwu. Evaluating the effect of speed and payload on robot repeatability. In "Robotics and computer-Integrated Manufacturing volr8", number 1, pages 27–33 (1991).

[10] Einar Ramsli. Probability distribution of repeatability of industrial robots. In "The International Journal of Robotics Research vol.10", number 3, pages 276–283 (1991).

[11] Raziel Riemer and Yael Edan. Evaluation of influence of target location on robot repeatability. In "Robotica", volume 18, pages 443–449 (2000).

[12] Y.L. Tong. "The multivariate normal distribution". Springer-Verlag (1988).